DOI: 10.24996/ijs.2024.65.5.12

ISSN: 0067-2904

Characterization Study of Neodymium Doped Tin Oxide Films for Optoelectronic Applications

Suhad A. Hamdan
Department of Physic, College of science, University of Baghdad, Baghdad, Iraq

Received: 1/1/2023 Accepted: 9/5/2023 Published: 30/5/2024

Abstract

Tin chloride of 1M concentration was used as the precursor, and neodymium chloride was used as a dopant (with different doping ratios) to create pure and neodymium (Nd) doped tin oxide (SnO_2) thin films with varied doping ratios (1, 3 and 5) wt%. Using UV-visible absorbance and XRD patterns, it was possible to analyze the impact of Nd doping ratio on the optical and structural characteristics of the produced thin films. All samples have a polycrystalline structure that is identical to the conventional SnO_2 peaks, according to XRD measurements. As the doping ratio rises, the crystallinity falls. At doping ratio of 5wt%, a new phase emerged for Nd_2O_3. According to optical characteristics, the transmittance rises with doping ratio, from 4.13% to 35.76% at 550 nm. The optical band gap increases from 3.60 to 4.20eV with an increase in Nd content from 0 to 5%, and the energy gap was a direct transition. I-V properties for all samples are examined in dark and light conditions. Photocurrent and dark current increases with increasing doping ratio. The produced films have shown increase in photoconductivity gain.

Keywords: tin oxide nanoparticles, spray paralysis preparation, optical properties, photoconductive, photoconductive gain.

دراسة توصيف أغشية أكسيد القصدير المشوبة بالنيوديميوم للتطبيقات الكهروضوئية

سهاد عبد الكريم حمدان
قسم الفيزياء، كلية العلوم، جامعة بغداد، بغداد، العراق

الخلاصة

تم استخدام كلوريد القصدير كمادة اولية بتركيز 1مولاري ، وتم استخدام كلوريد النيوديميوم كمشوب بالنسب المختارة لإنشاء أغشية رقيقة نقية وأكسيد القصدير (SnO_2) شوب (Nd) بنسب متنوعة (1 ، 3، 5) بالوزن٪. باستخدام الامتصاص المرئي للأشعة فوق البنفسجية و XRD ، كان من الممكن تحليل تأثير نسبة التشويب Nd على الخصائص البصرية والهيكلية للأغشية الرقيقة المنتجة. تحتوي جميع العينات على هيكل متعدد البلورات مطابق لقمم SnO_2 التقليدية ، وفقًا لقياسات XRD. مع ارتفاع نسبة التشويب ، تنخفض التبلور.

عند نسبة التشويب 5٪ بالوزن ظهر طور جديدة لـ Nd_2O_3. وفقًا للخصائص البصرية ، ترتفع نسبة النفاذية من 4.13٪ إلى قيم 35.76٪ عند 550 نانومتر. تزداد فجوة النطاق البصري من 3.60 إلى 4.20 الكترون فولت مع زيادة محتوى Nd من 0 إلى 5٪ ، وكانت فجوة الطاقة عبارة عن انتقال مباشر. تم فحص خصائص

*Email: suhad.a@sc.uobaghdad.edu.iq

I–V لجميع العينات في كل من الظروف المظلمة والمضيئة. زاد التيار الضوئي والتيار المظلم مع زيادة التشويب . أظهرت الأفلام المنتجة زيادات في كسب الموصلية الضوئية.

1. Introduction

An essential material of tin chemistry is tin (IV) oxide, an inorganic compound with the formula SnO_2. It is an amphoteric solid that is diamagnetic and colorless, with a rutile structure [1]; the oxygen atoms are 3 coordinates while the tin atoms are 6 coordinates [2]. Figure 1 shows how SnO_2 is structured [3].

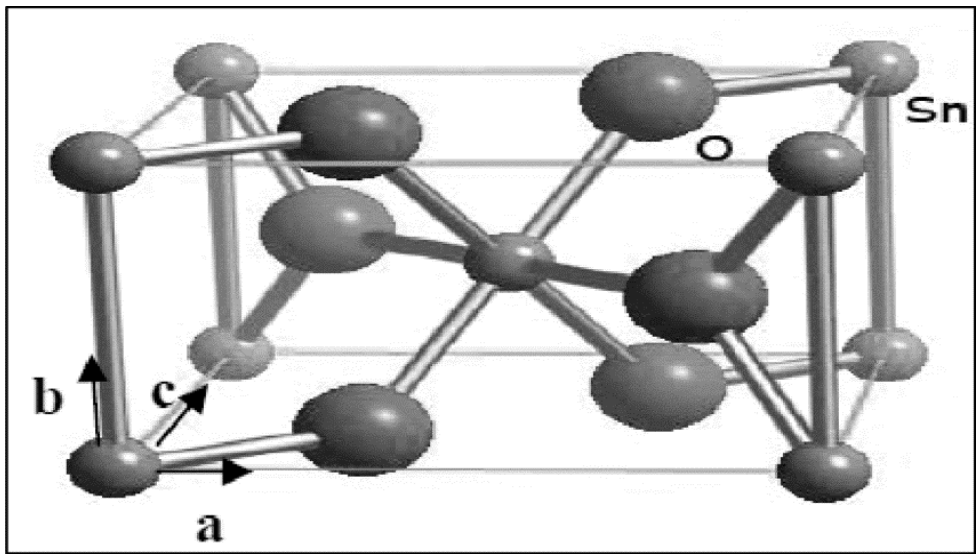

Figure 1: The structure of SnO_2 [3]

SnO_2 can be defined as an n-type semiconductor with low electrical resistance and high optical transparency in the visible region of the electromagnetic spectrum. Due to such characteristics, tin oxide is excellent for numerous applications [4]. SnO_2 is a crucial Transparent Conducting Oxide (TCO) which is used in many different fields, including solar cells, gas sensors, and optoelectronic and heat-mirror devices [5]. Undoped and doped tin oxide thin films were the subject of several studies utilizing a variety of production processes, including spray pyrolysis [6], chemical vapor deposition [7], radio frequency sputtering [5], pulse laser deposition [8], etc. Tin (IV) oxide has historically been utilized in various fields, including ceramic glazes [9]. When combined with lead oxide, tin (IV) oxide could be utilized as a polishing powder for glass, marble, jewellery, and silver [10]. SnO_2 could be employed in high voltage varistors, gas sensing, glass coating, and doping with cobalt and manganese [11]. SnO_2 has grown in importance in optoelectronic devices due to its high electron mobility and stability. SnO_2 is commonly employed as a UV photodetector because it is an oxide semiconductor with a large bandgap of about 3.6 eV [12]. Therefore, the impact of Nd doped SnO_2 films with various doping ratios was previously researched by multiple researchers [13] [14] [15], and it was found that doping with Nd improves the properties of SnO_2.

The work's objective is to study the effect of doping with Nd on the structural and optical characteristics of SnO_2 thin films produced by spray pyrolysis. An SnO_2 photoconductive detector was created to analyze the variation in Nd content during thin film production.

2. Experimental work

The production of tin oxide doped with Nd required using neodymium chloride ($NdCl_2$) as a source of Nd dopant and tin chloride ($SnCl_2$) as a source of tin. A distilled water was

utilized as the solvent. Thin films, using the spray pyrolysis method, were deposited on glass and silicon substrates which were kept at a temperature of 250^{o}C. Thin films of SnO_2 doped with (0, 1, 3 and 5) wt% Nd were prepared. The spray pyrolysis is a chemical process that involves spraying a solution onto a substrate that has been heated to 250°C, in which the solution reacts to generate an oxide film. The spray rate of the solution was modified to 5 sprinkles per min., with each sprinkle lasting roughly 10 sec. The spray nozzle-substrate distance was 30cm. The carrier gas utilized was oxygen. A thermocouple was used to regulate the substrate's temperature. The weighing method was used to determine the films' thickness (t).

Different techniques were utilized to assess the thin films. An XRD apparatus of SHIMADZU type was utilized to examine the structure regarding the Nd-doped SnO_2 thin film. The voltage was 40kV, and the current was 30mA for the X-ray source with the Cu target of the (Kα) transition with wavelength λ= 1.5405 Å. The scanning angle 2θ was in the range (20˚-80̊). The optical characteristics of pure and Nd-doped SnO_2 thin films were studied with a UV-Visible spectrometer (UV mini1240) with a wavelength range of (300-1100) nm. This device is a single-beam model. After normalizing the sample with a clean slide, the measurement technique depends on transmission through the sample. IV measurements were performed using a 100 mW/cm^2 Philips Halogen lamp, a D.C. power supply, a Keithly digital electrometer 616.

3. Results and discussion

Figure (2) depicts the XRD patterns for pure and Nd-doped SnO_2 thin films deposited on glass substrates. All X-ray patterns indicated a polycrystalline structure. The diffraction peaks located at (26.4605˚, 33.7457˚, 38.0069˚, 51.6151˚, and 65.0172˚) for the pure sample were identical with the standard card No. 96-500-0225 for tetragonal SnO_2 corresponding to (110), (101), (200), (211) and (112) planes, respectively. The peaks intensity decreased with increasing the doping ratio. Full widths at half-maximum (FWHM) increase indicates the reduction of the crystalline size, which can be evaluated using Scherer's formula [16]:

$$D = \frac{K\lambda}{\beta cos\theta} \quad (1)$$

D represents the average crystalline size, K=0.9 is the shape factor, λ represents XRD wavelength, β is the FWHM of the diffraction peak (in radians), and θ represents Bragg diffraction angle. The following equation is Bragg's law establishes the conditions necessary for diffractions from various planes [17]:

$$2d_{hkl}sin\theta = n\lambda \quad (2)$$

Where: n = 1, 2, 3,... is an integer that typically has the value of n = 1, d represents the spacing between the planes, θ is the angle of the X-ray beam with the plane, and λ represents the wavelength of the X-ray. With card number 96-101-0282, an additional phase is seen with a greater doping ratio and is identical to hexagonal Nd_2O_3. The XRD parameters are displayed in Table (1). Since the radius of Nd^{3+} (0.099 nm) is not significantly larger than that of Sn^{4+} (0.071 nm), it is possible for Nd^{3+} ions to collaborate with the matrix of SnO_2 particles to produce Nd-Sn-O solid solutions. Due to the difference in ionic radius between the atoms of the host and dopant, the doping of a host matrix by various ions might alter the lattice properties [13].

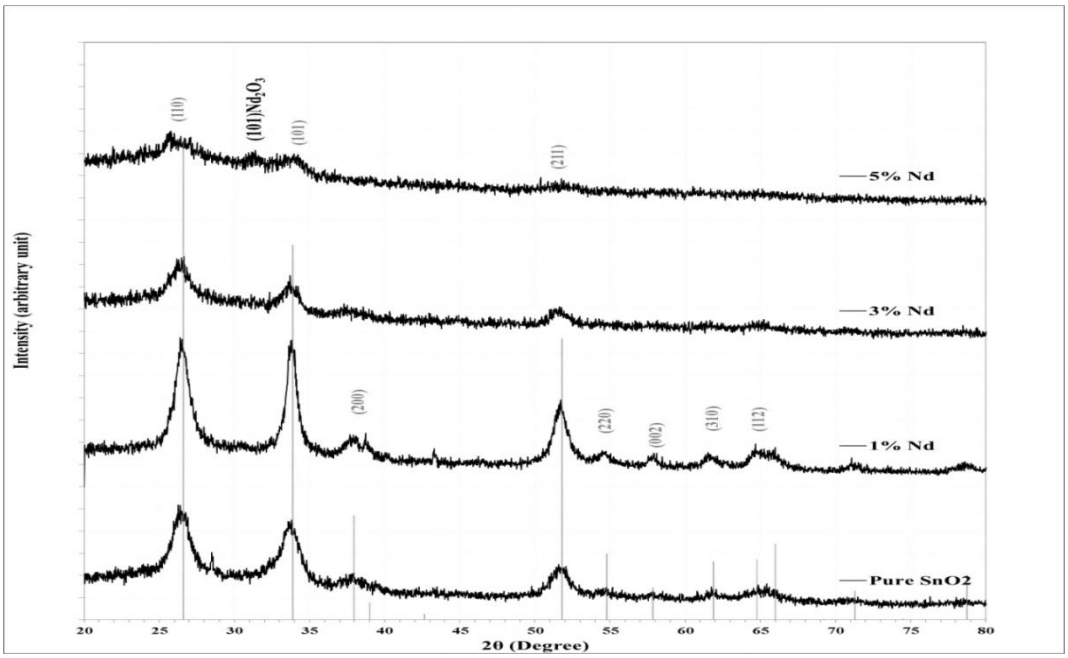

Figure 2: XRD patterns for Nd doped SnO_2 films at various doping ratios

Table 1: Structural parameters: 2θ, (hkl), d_{hkl}, FWHM and C.S for Nd doped SnO_2 films at various doping ratios

Nd%	2 θ (deg.)	FWHM (deg.)	D_{hkl} exp.(å)	c.s (nm)	D_{hkl} std.(å)	Phase	hkl	Card no.
	26.4605	1.3058	3.3657	6.2	3.3496	Tet.SnO_2	(110)	96-500-0225
	33.7457	1.4433	2.6539	5.8	2.6431	Tet.SnO_2	(101)	96-500-0225
0	38.0069	1.3058	2.3656	6.4	2.3685	Tet.SnO_2	(200)	96-500-0225
	51.6151	1.5808	1.7694	5.6	1.7639	Tet.SnO_2	(211)	96-500-0225
	65.0172	2.1306	1.4333	4.4	1.4382	Tet.SnO_2	(112)	96-500-0225
	26.4605	1.2371	3.3657	6.6	3.3496	Tet.SnO_2	(110)	96-500-0225
	33.8144	0.8247	2.6487	10.1	2.6431	Tet.SnO_2	(101)	96-500-0225
	38.0756	1.2371	2.3615	6.8	2.3685	Tet.SnO_2	(200)	96-500-0225
1	51.7526	1.0997	1.7650	8.0	1.7639	Tet.SnO_2	(211)	96-500-0225
	54.6392	1.0309	1.6784	8.7	1.6748	Tet.SnO_2	(220)	96-500-0225
	58.0069	1.0309	1.5887	8.8	1.5925	Tet.SnO_2	(002)	96-500-0225
	61.5120	0.9622	1.5063	9.6	1.4980	Tet.SnO_2	(310)	96-500-0225
	64.6048	1.3745	1.4415	6.8	1.4382	Tet.SnO_2	(112)	96-500-0225
	26.3918	1.8557	3.3743	4.4	3.3496	Tet.SnO_2	(110)	96-500-0225
3	33.5395	1.7870	2.6698	4.6	2.6431	Tet.SnO_2	(101)	96-500-0225
	51.5464	1.9244	1.7716	4.6	1.7639	Tet.SnO_2	(211)	96-500-0225
	26.4605	1.7800	3.3657	4.6	3.3496	Tet.SnO_2	(110)	96-500-0225
5	**31.1900**	**1.2100**	**2.8653**	**6.8**	**2.9098**	**Hex.Nd_2O_3**	**(101)**	**96-101-0282**
	34.1581	1.6495	2.6228	5.0	2.6431	Tet.SnO_2	(101)	96-500-0225
	51.9588	1.4433	1.7585	6.1	1.7639	Tet.SnO_2	(211)	96-500-0225

The interaction between electromagnetic radiation with semiconductors is characterized by the optical constants, which are: extinction coefficient (k), refractive index (n), and real (ε_r) and imaginary (εi) parts of the dielectric constant. Measurements of values and variables of

optical constant over a range of energy provide information on those fundamental characteristics such as band structure of the material or impurities in the crystals. Detailed and accurate knowledge of optical constant are also required in such practical applications as design of lens system, second harmonic generation and fiber optics [18]. The optical characteristics involve optical transmittance, the optical energy gap (E_g^{opt}), absorption coefficient, and optical constants (n, k, ε_r and εi).

The transmission spectra for Nd-doped SnO_2 thin films on glass substrate at different doping ratios in the wavelength range (300nm-1100nm) were determined by UV-visible spectroscopy, as exhibited in Figure (3). It seems that transmission increased with increasing the doping ratio of Nd; this may be due to the increase of the band gap energy with the decrease of crystallinity.

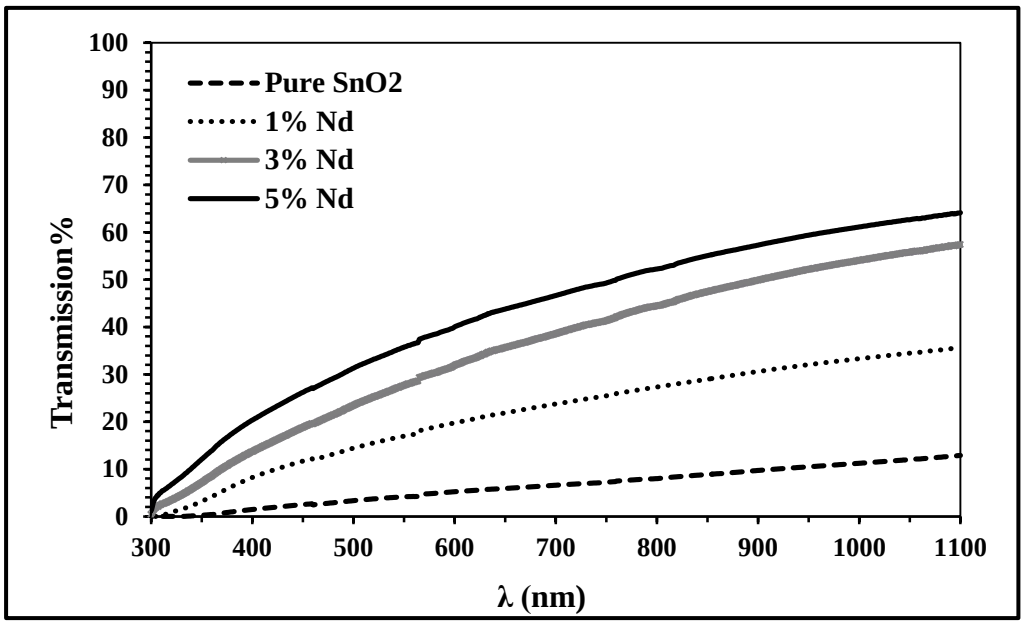

Figure 3: Transmission spectra as a wavelength function for Nd doped SnO_2 films at different doping ratios

The absorption coefficient for Nd-doped SnO_2 thin films deposited on glass substrates was determined by the following equation:

$$I = I_o e^{-\alpha t} \tag{3}$$

Where: I_o and I are the incident and transmitted photon intensity, respectively, α represents the coefficient of absorption, defined as the relative number of photons that are absorbed per unit distance of the semi-conductor, and t represents material thickness [19], [20]. The variations of the absorption coefficient with wavelength for different doping ratios are shown in Figure (4). the absorption spectra generally have the opposite behavior of that of the transmission spectra
, i.e. decrease with the increase of the doping ratio. The absorption coefficient values in the range of 10^4 cm^{-1} indicate direct transition.

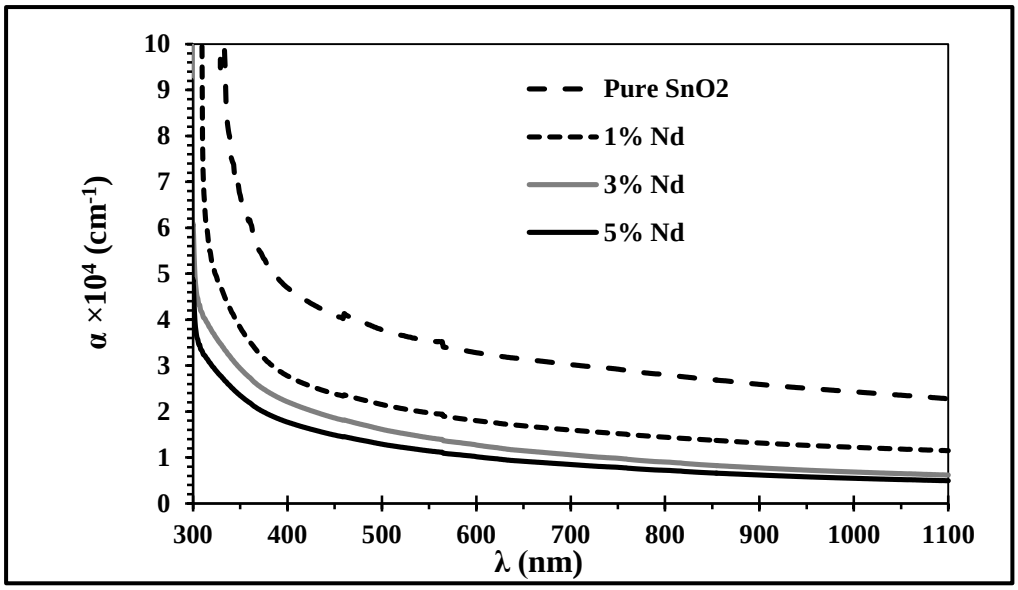

Figure 4: Variation of absorption coefficient with wavelength for Nd-doped SnO_2 films at different doping ratios

The energy band gap energy depends on the films crystallinity and the crystalline size. The values of the optical energy gap (E_g^{opt}) for films were determined by the use of Tauc formula [21]:

$$\alpha h\nu = B(h\nu - E_{opt})^r \quad (4)$$

Where: B represents a constant, r=1/2, 2, 3/2, 3 for allowed direct, allowed indirect, forbidden direct, and forbidden indirect transitions, respectively.

The energy gap was measured from the intercept with the x-axis of the extrapolated linear part of the curve. The Tauc plots of Pure and Nd-doped samples are illustrated in Figure5. Table 2 shows the obtained values of the band gap energies. It can be noted that the energy gap increases from 3.6 to 4.2eV with the increase in the Nd doping ratio, which may be due to the decrease of the crystalline size due to the electron confinement effect [22]. The values of the energy gap were higher than the reported values of bulk SnO_2 of 3.6 eV [23] [24] [25].

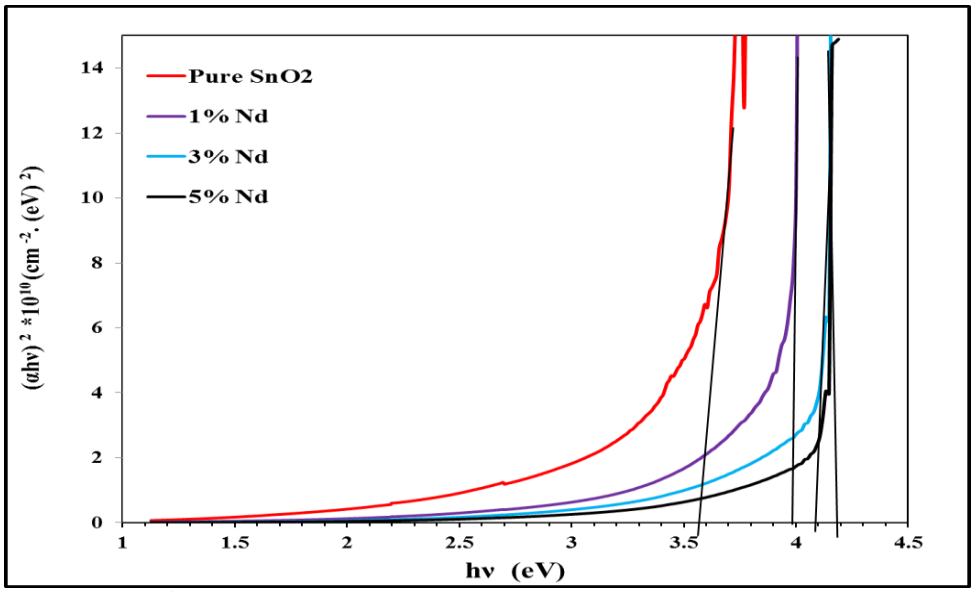

Figure 5: $(\alpha h\nu)^2$ as a function of hν for Nd doped SnO_2 films at various doping ratios

The refractive index, dielectric constants, extinction coefficient, and dielectric loss were calculated for all samples at λ=550 nm, as shown in Table (2). The value of the refractive index (n) may be calculated from the following formula [26]:

$$n = \left(\frac{4R}{(R-1)^2} - k^2\right)^{1/2} - \frac{(R+1)}{(R-1)} \quad (5)$$

The coefficient of extinction is related to the coefficient of absorption α by the equation [27]:

$$k = \alpha\lambda / 4\pi \quad (6)$$

The real ε_r and imaginary ε_i parts of the dielectric constant are calculated as follows [27]:

$$\text{Complex refractive index } N^* = n - ik \quad (7)$$

$$\text{Complex dielectric constant } \varepsilon^* = \varepsilon_r - i\varepsilon_i \quad (8)$$

From the relation $N^* = \sqrt{\in *}$, thus:

$$\varepsilon_r = n^2 - k^2 \quad (9)$$

$$\varepsilon_i = 2nk \quad (10)$$

The table shows that the refractive index decreased with increasing the Nd doping ratio from 0 to 5%, which could be a result of changes in bond length as a result of decreasing packing density with the reduction of crystallinity. The coefficient of extinction (k) decreased, corresponding to the decrease in the absorption coefficient. The behavior of the real dielectric constant (ε_r) was similar to that of the refractive index, while the imaginary dielectric constant (ε_i) mainly depended upon the k values, related to the variation of the absorption coefficient. Both ε_r and ε_i decreased with increasing the doping ratio.

Table 2: Optical constants at λ= 550 nm for Nd doped SnO_2 films at different doping ratios

Nd%	T%	α (cm^{-1})	K	n	ε_r	ε_i	Eg (eV)
0	4.13	35405	0.155	3.658	13.356	1.134	3.60
1	16.98	19698	0.086	3.695	13.649	0.638	4.00
3	27.66	14281	0.063	3.419	11.689	0.428	4.10
5	35.76	11425	0.050	3.176	10.087	0.318	4.20

For making a photodetector, aluminum (Al) electrodes of 100 nm thickness were thermally evaporated and deposited on top of SnO_2: Nd thin films at room temperature using a metal mask. Figure (6) shows the relationship between dark current (I_d) and applied voltage for undoped and doped SnO_2 films at voltage bias (0-3) V. This figure demonstrates how the dark current rises with increasing the voltage bias. The probability of capturing free charge carriers through recombination and capture centers that result from adding Nd increased at low voltage (0-1.5 volt), causes an increase in the transit time (t_r) between the electrodes and a decrease in mobility and drift velocity. Thus, the increase in dark current was minimal at these low voltages. However, when the applied electric field on the detector was raised, i.e. at high voltage (V>1.5 volt), the drift velocity increased. As a result, the defects become ineffective, reducing transit time and changing the dark current behavior to become linear as a function of the high voltage bias. Figure (6) shows the IV characteristics for all samples, which demonstrate Schottky junction behavior of all samples, while for 0%Nd, the ohmic contact is behavior prominent. The rise in dark current is partly caused by an increase in the number of free carriers (electrons and holes) and partially by a reduction in the potential barrier at the

grain boundaries, which improves carrier mobility at the grain boundaries and boosts the carriers' photoconductivity [28].

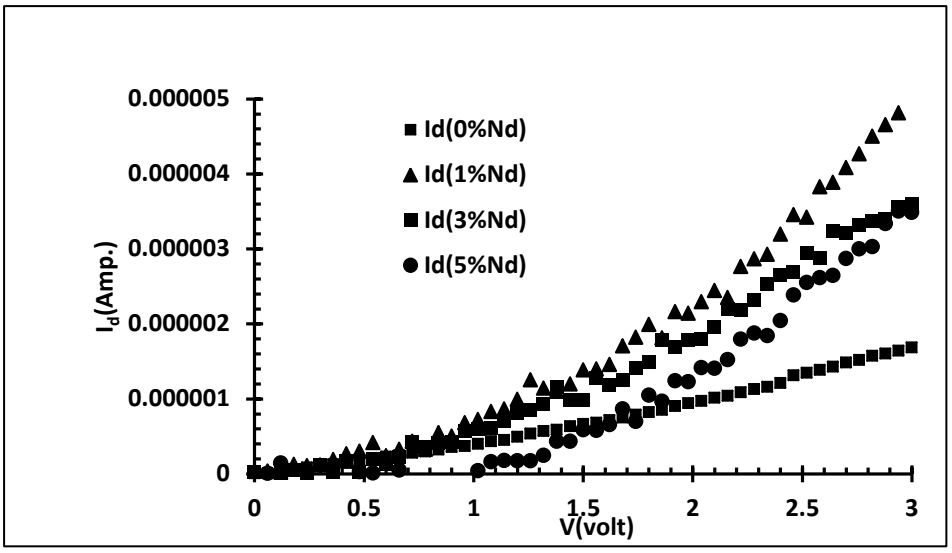

Figure 6: The relation between dark current and applied voltage for undoped SnO_2 films and doped with (1,3,5)wt.%Nd

Figure (7) shows the relation between photocurrent and applied voltage for undoped and doped SnO_2 thin films at voltage bias (0-3) V measured under illumination by 100 mW/cm^2 Halogen lamp. The photocurrent is an important parameter which plays an effective role in photodetectors and solar cells. The increase of photocurrent with increasing the Nd content means positive photoconductivity. The photocurrent increased with increasing the Nd content, and then decreased at the high value of Nd content, as shown in Table (3). This is explained by the fact that increasing the Nd content creates sensitizing centers inside the energy gap accountable for the generation and recombination processes; increasing the sensitizing center and free charge carrier leads to an increase in photocurrent. At high values of the Nd content, all effective and recombination centers are filled, causing all free charge carriers to transfer and extinguish, resulting in a reduction in photocurrent.

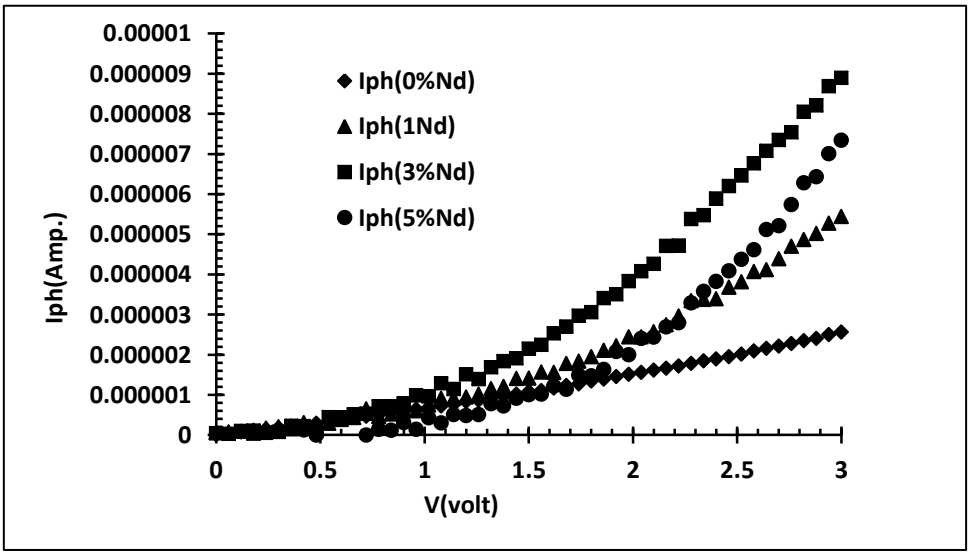

Figure 7: The relation between current and applied voltage for undoped SnO_2 and doped with (1, 3, 5) wt. % of Nd under illumination

Figure(8) illustrates the relation between photocurrent and dark current for undoped SnO_2 and doped with ratio (1, 3, and 5) wt. % of Nd.

The photoconductive gain (G) is the ratio between photocurrent and dark current (I_{ph}/I_d) at the same bias voltage [29], and it is about 1.524, 3.174, 2.75, 2.107 for (0, 1, 3, 5) wt.%Nd, respectively at 3V as shown in Table (3).

The thin film dopant with 1%Nd has a maximum G value of 3.174. From these results, it can be concluded that the device prepared from thin films doped with different doping ratios of Nd exhibited the best characteristics for photodetector applications.

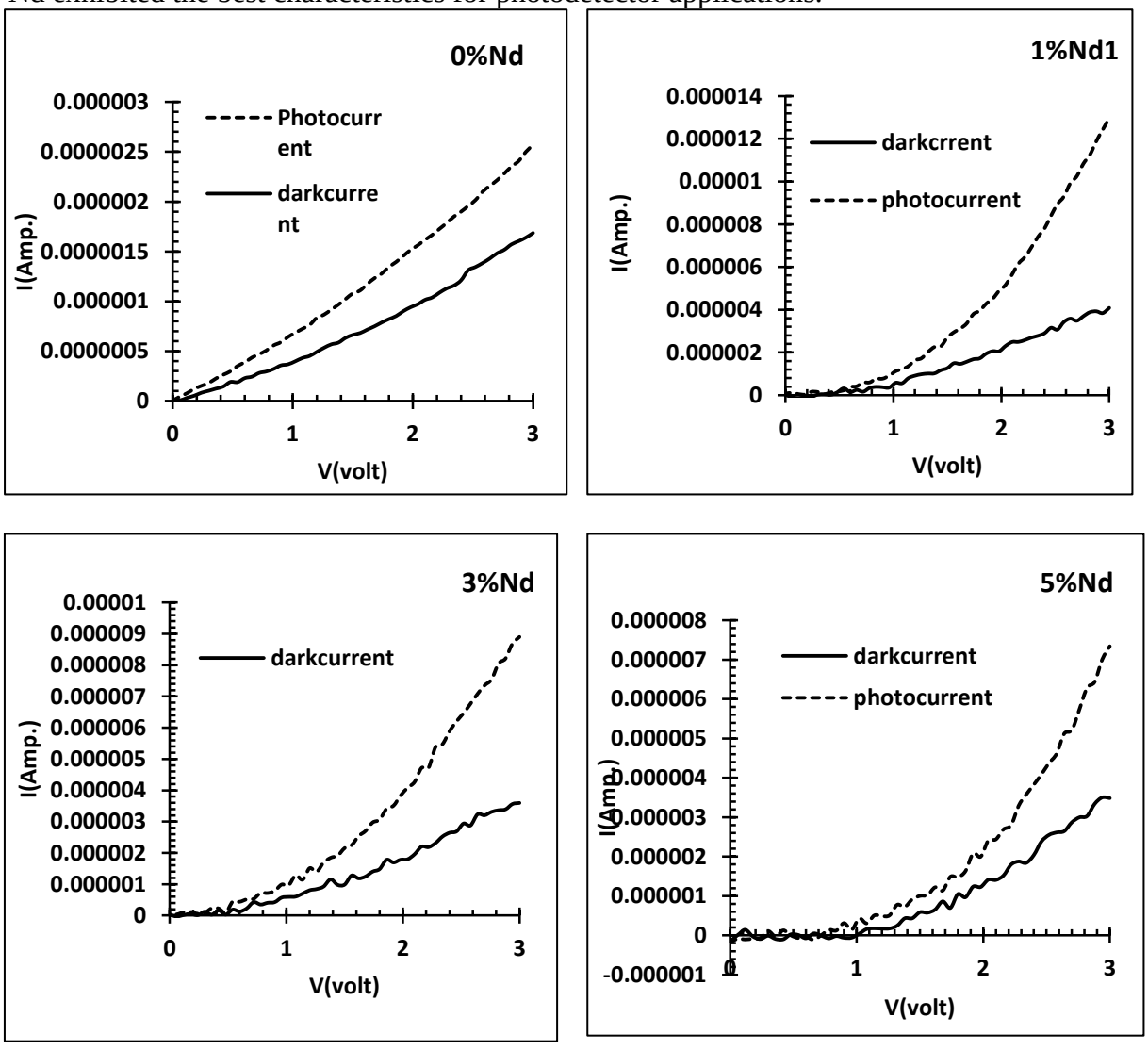

Figure 8: The relation between current and applied voltage for undoped SnO_2 and doped with ratio (1, 3, 5) wt. % of Nd under dark and illumination

Table 3: gain at 3 volt for Nd doped SnO_2 films at different doping ratios

Nd%	I_{ph}(amp.)At 3 volt	I_d (amp.)At 3 volt	Gain at 3 volt
0	0.256893E-05	1.68558E-06	1.524
1	1.29687 E-05	4.08563E-06	3.174
3	89.0117 E-05	3.5915E-06	2.475
5	73.4211 E-05	3.4842E-06	2.107

4. Conclusions

Pure SnO_2 thin film and doped with Nd at different ratios were successfully prepared by spray pyrolysis technique. Structural study illustrated polycrystalline structure for all thin films. The crystallinity and the average crystalline size decrease with increasing the Nd doping ratio from 0 to 5wt.%. A new phase appeared at the 5% Nd doping ratio corresponding to Hexagonal Nd_2O_3 structure. Thin film had high optical transmittance in the visible region, and the transmission increased with increasing the Nd ratio. The energy gap for the prepared thin films increased from 3.6 to 4.2 eV with increasing Nd content from 0 to 5%. An increase of positive photoconductivity was observed in the prepared films.

References

[1] J. W. G.J. McCarthy and G. M. J. M. McCarthy, Welton, "X-Ray Diffraction Data for SnO_2. An Illustration of the New Powder Data Evaluation Methods," *Powder Diffraction*, vol. 4, pp. 156-159, 1989.

[2] J.G. Zheng, X. Pan, M. Schweizer, F. Zhou, U. Weimar, W. Göpel, M. Rühle, "Growth twins in nanocrystalline SnO2 thin films by high-resolution transmission electron microscopy," *J. Appl. Phys.*, vol. 79, pp. 7688-7694, 1996.

[3] A. Norman N. Earnshaw, Chemistry of the Elements, Oxford: Pergamum Press, p. 447–48, 1984.

[4] X.Q. Pan, L. Fu, "Oxidation and phase transitions of epitaxial tin oxide thin films on (012)(1̄012) sapphire," *J. Appl. Phys.*, vol. 89, pp. 6048-6055, 2001.

[5] S. Baco, A. Chik, and F. Md. Yassin, "S. Baco, A. Chik, and F. Md. Yassin, "Study on Optical Properties of Tin Oxide Thin Film at Different Annealing Temperature," *J. Sci. Technol,* vol. 4, p. 61–72, 2012.

[6] L. Filipovic and S. Selberherr, "Performance and Stress Analysis of Metal Oxide Films for CMOS-Integrated Gas Sensors," *Sensors*, vol. 15, pp. 7206–7227, 2015.

[7] S. M. Ali, S. T. Hussain, S. A. Bakar, J. Muhammad, and N. ur Rehman, "Effect of doping on the Structural and Optical Properties of SnO2 Thin Films fabricated by Aerosol Assisted Chemical Vapor Deposition," *J. Phys. Conf. Ser., vol. 439, p. 012013, 2013.*

[8] G. Korotcenkov, S. H. Han, and B. K. Cho, "Material Design for Metal Oxide Chemiresistive Gas Sensors," *J. Sens. Sci. Technol.*, vol. 22, no. 1, pp. 1-17, 2013.

[9] S. Subramanian, R. Valantina, and C. Ramanathan, "Structural and electronic properties of CuO, CuO_2 and Cu_2O nanoclusters – A DFT approach," *Medziagotyra*, vol. 21, no. 2, pp. 173–178, 2015.

[10] S. Krishna, Handbook of Thin-Film Deposition Processes and Techniques, New York: William Andrew Publishing, 2002.

[11] R. T. Jacob, J. Thomas, R. George, and M. Kumaran, "Comparative study on ammonia sensing properties of SnO2 nanocomposites fabricated via electrospinning and sol-gel process," *Int. J. Res. Eng. Technol*., vol. 3, pp. 599–605, 2014.

[12] Yong Zhang, Wenxin Xu, Xiaojie Xu, Jian Cai, Wei Yang, and Xiaosheng Fang, " Self-Powered Dual-Color UV−Green Photodetectors Based on SnO2 Millimeter Wire and Microwires/CsPbBr3 Particle Heterojunctions," *The Journal of Physical Chemistry Letters*, vol. 10, no. 4, pp. 836-841, 2019.

[13] WU Shide, LI Chao, WEI Wei, WANG Huanxin, SONG Yanliang, ZHU Youqi, LU lingzhen, "Characterization and its gas sensing property," *Journal of Rare Earths*, vol. 28, Spec. Issue, p. 171, 2010.

[14] G. Turgut, E. Sonmez, S. Duman,"Evaluation of an Nd Doping Effect on Characteristic Properties of Tin Oxide," *Mate. Sci. in Semi. Pro.*, vol. 30, pp. 233-41,2015.

[15] Sachin T. Bahade, Amrut S. Lanje, Satish J. Sharma, "Effect of Nd doping on Structural & Optical Properties SnO2 Nanorods Science," *Science, Technology and Development*, vol. X, no.

II, pp. 323-328, 2021.

[16] S. A. Hamdan, I. M. Ibrahim, I. M. Ali, "Comparison of Anatase and Rutile TiO2 Nanostructure for Gas Sensing Application," *Digest Journal of Nanomaterials and Biostructures, v*ol. 15, no. 4, pp. 1001-1008, 2020.

[17] Suhad A. Hamdan, Iftikhar M. Ali, "Enhancement of Hydrothermally Co_3O_4 Thin Films as H_2S Gas Sensor by Loading Yttrium Element," *Baghdad Science Journal*, vol. 16, no. 1 (Suppl.), pp. 221-229, 2019.

[18] J. S. Blakemore, "Solid State Physics", 2nd ed., W. B. Saunders Company, Philadelphia, (1974).

[19] R. E. a. A.I.Gibson, An Introduction to Solid State Physics and Application, 1st ed., Macillian Inc., 1974.

[20] R. Elliot and A.I.Gibson, An Introduction to Solid State Physics and Application, 1st ed., Macillian Inc., 1974.

[21] Ikram Kamel abd Karem, Suhad A. Hamdan, "The Influence of CeO2 Concentration on Some Physical Properties of Y2O3 Thin Films," *Iraqi Journal of Science*, vol. 63, no. 6, pp. 2482-2491, 2022.

[22] Rolf Koole, Esther Groeneveld, Daniel Vanmaekelbergh, Andries Meijerink and Celso de Mello Donegá, "Size Effects on Semiconductor Nanoparticles", In: de Mello Donegá, C. (eds) Nanoparticles. Springer, Berlin, Heidelberg, 2014

[23] S. T. Bahade, A. S. Lanje, S. J. Sharma, "Synthesis of SnO2 Thin Film by Sol gel Spin Coating Technique for Optical and Ethanol Gas Sensing Application," *J. Sci. Res. in Scientific Tech.*, vol. 3, no. 7, pp. 567-575, 2017.

[24] A. S. Lanje, S. J. Shrama and R. B. Pode, "Functional Nanomaterials Synthesis and Characterization", LAMBERT Aca.Pub., Germany 2014.

[25] S. T. Bahade, A. S. Lanje, S. J. Sharma and A. I. Prasad, "Influence of Ceria Doping on Structural and Optical Properties of Tin Oxide Nanoparticles", *IJCESR*, vol. 5, no. 1, pp. 235-241, 2018.

[26] B. Ray, [II-VI Compounds], Pergamon Press, 1st edition printed, Great Britain , Ne and Co. Ltd. of Edinburgh, p.162, 1969.

[27] S. M. Sze and K. K. Ng, Physics of Semiconductor Devices. 2007.

[28] E. M. Nasir, M. M. Abass, "Optical and Photoconductive Properties of Chemically Deposited Nanocrystalline PbS Thin Films," *Chalcogenide Letters*, vol. 16, no. 8, pp. 409 - 415, 2019.

[29] S.K.J. Al-Ani, H.H. Mohammed, E.M.N. Al-Fwade, "The optoelectronic properties of CdSe:Cu photoconductive detector," The Energy for the 21st Century World Renewable Energy Congress VI 1–7 July 2000 Brighton, UK, 2000, Pages 2026-2031